Polymer Chemistry

ROYAL SOCIETY OF CHEMISTRY

PAPER

View Article Online
View Journal | View Issue

Cite this: *Polym. Chem.*, 2022, **13**, 6061

Surface-initiated reversible addition fragmentation chain transfer of fluoromonomers: an efficient tool to improve interfacial adhesion in piezoelectric composites†

Vincent Bouad,[a,b] Kohji Ohno,[c] Ahmed Addad,[b] Adeline Marin,[b] Nicolas Donzel,[a] Sophie Barrau,*[b] Joël Lyskawa*[b] and Vincent Ladmiral*[a]

This article reports the surface-initiated Reversible Addition–Fragmentation chain Transfer polymerization (SI-RAFT) of trifluoroethylene (TrFE) and vinylidene fluoride (VDF) from barium titanate nanoparticles (BTO NPs) for the preparation of piezoelectric composites. A new xanthate chain transfer agent (DOPA-XA) derived from *O*-ethyl-*S*-(1-methoxy-carbonyl) ethyldithiocarbonate and integrating a catechol moiety able to efficiently bind onto the BTO NP surface was synthesized, characterized *via* ^{1}H and ^{13}C NMR spectroscopy and employed to mediate SI-RAFT polymerizations. This DOPA-XA was immobilized onto BTO NPs and the grafting efficiency was evaluated by TEM images and XPS measurements while the grafting density (Γ > 0.2 chains per nm^2) was calculated using TGA and BET measurements. Poly(trifluoroethylene)- (PTrFE) and poly(vinylidene fluoride-*co*-trifluoroethylene)- (P(VDF-*co*-TrFE) functionalized BTO NPs were prepared by SI-RAFT polymerization and characterized by nuclear magnetic resonance (NMR), size exclusion chromatography (SEC), thermogravimetric analysis (TGA), transmission electron macroscopy (TEM) and X-ray photoelectron microscopy (XPS). Interestingly, polymer brushes featuring relatively low dispersities ($Đ$ < 1.5) and high grafting densities (Γ > 0.2 chains per nm^2) were obtained. Piezoelectric composite films were then prepared from these fluoropolymer-decorated BTO NPs by incorporation into a P(VDF-*co*-TrFE) matrix using the solvent casting method. The homogeneity of the NPs dispersion in the copolymer matrix was assessed by SEM and the direct piezoelectric response of the composites was recorded after polarization and compared with composites prepared from non-modified BTO NPs. The measured piezoelectric coefficients (d_{33}) of all the composites were of the same order of magnitude (around −9 pC N^{-1}). Finally, the interface between the NPs and the copolymer matrix was mechanically stressed by stretching. The SEM images of the composite fracture showed, in the case of nongrafted BTO NPs, the presence of cavities close to the NPs associated with a weak interfacial adhesion while, for fluoropolymers grafted BTO NPs, the interface with the copolymer matrix was cohesive. This study leads to innovative composites with a cohesive ceramic/polymer interface for piezoelectric applications.

Received 25th June 2022,
Accepted 9th October 2022

DOI: 10.1039/d2py00825d

rsc.li/polymers

Introduction

Since the discovery of piezoelectricity in 1880 by Curie *et al.*,[1] piezoelectric behaviour have been found in various materials such as natural crystals, ceramics and polymers. Piezoelectric ceramics such as Pb[Zr$_x$Ti$_{1-x}$]O$_3$ (PZT, Lead Zirconate Titanate),[2] BaTiO$_3$ (BTO, Barium Titanate)[3] or Bi$_{0.5}$Na$_{0.5}$TiO$_3$ (BNT, Bismuth Sodium Titanate)[4] are piezoelectric materials exhibiting very high piezoelectric coefficienst (d_{33} up to 500 pC N^{-1} for PZT[5]). PZT, a piezoelectric ceramic with the highest piezoelectric response, has been widely used as an actuator or as an ultrasonic transducer.[6,7] However, it contains harmful elements such as lead that dramatically limits its use. Therefore, BNT and BTO are progressively used to replace PZT. Nevertheless, in spite of their high piezoelectric coefficient, piezoelectric ceramics suffer from stiffness which may limit their applications in devices which require flexibility or complex shapes.

The incorporation of piezoelectric nanoparticles in a polymer matrix enabled the preparation of flexible composite

[a]*ICGM, University of Montpellier, CNRS, ENSCM, Montpellier, France. E-mail: vincent.ladmiral@enscm.fr*
[b]*Université de Lille, CNRS, INRAE, Centrale Lille, UMR 8207 – UMET – Unité Matériaux et Transformations, F-59000 Lille, France. E-mail: joel.lyskawa@univ-lille.fr, sophie.barrau@univ-lille.fr*
[c]*Department of Materials Science, Graduate School of Engineering, Osaka Metropolitan University, Sakai, Osaka 599-8531, Japan*
† Electronic supplementary information (ESI) available. See DOI: https://doi.org/10.1039/d2py00825d

materials with high piezoelectric properties.[8,9] The first attempts to prepare such piezoelectric composites was reported by Kitayama and Sugawara who incorporated PZT nanoparticles in a polyurethane matrix.[10]

In this context, since the discovery of piezoelectricity in polymers such as poly(vinylidene fluoride) (PVDF) by Kawai in 1969,[11] piezoelectric composites integrating an active polymer matrix (*i.e.* a piezoelectric polymer matrix) have shown growing interests. Indeed, PVDF and several other fluorocopolymers are semi-crystalline and belong to the ferroelectric polymers class since they display dipoles that can be oriented by an external electric field. These fluoropolymers possess the highest piezoelectric coefficient among polymers with values around −30 pC N^{-1}.[12] In addition, P(VDF-*co*-TrFE) copolymer (composed of VDF (vinylidene fluoride) and TrFE (trifluoroethylene)) presents the main advantage to directly crystallize in the electroactive crystal phase[13] contrary to the PVDF which requires, for instance, stretching[14–16] to form the polar phase[17,18] (*i.e.* the β-phase presenting the highest d_{33} compared to other crystal phases α,[17] δ,[17] γ[19] and ε[20]). Interestingly, P(VDF-*co*-TrFE) presents a d_{33} of −38 pC N^{-1},[21] which is relatively close to the value of pure PVDF β-phase. Currently, the main challenge in composites integrating fluoropolymer as polymer matrix and piezoelectric ceramics is to obtain materials with enhanced piezoelectric properties resulting from the cumulative effects of both components.[22,23] Because of the opposite signs of the piezoelectric coefficient d_{33} of the polymer (negative) and of the ceramic (positive), the main strategy to obtain cumulative effects consists in using anti-parallel poling.[22–24] However the limitation of piezoelectric properties of ceramic/fluoropolymers composites may also come from the poor affinity between the ceramic NPs and the fluoropolymers matrix potentially leading to the formation of cavities at the ceramic/polymer interface,[25] and ultimately to important dielectric losses which decrease the polarization of the composites.[26] To solve this problem, one attractive solution consists in the grafting of a coupling agent onto the nanoparticles surface to promote interfacial compatibility and adhesion by creating physico-chemical interactions between both constituents of the composite. Such coupling agents have two major roles in piezoelectric composites: (i) firstly, they modify the surface energy of the particles thus increasing their dispersibility in the solvent during the processing step based on the solvent casting method; (ii) secondly, they improve the dispersion of the ceramic particles in the polymer matrix and reinforce the ceramic/polymer interface. This better dispersion avoids the formation of aggregates and then prevents inhomogeneities in the composites thus improving their physico-chemical properties.[27–29] In this context, silanes,[30,31] dopamine, dopamine derivatives[32–34] and polydopamine[29,35] or other molecules capable of creating strong bonds[36–38] with both ceramic and polymer have been used as coupling agents.

To further enhance ceramic/polymer matrix interface, a promising approach consists in the direct grafting of polymers onto the ceramic surface. This grafting can be achieved by the functionalisation of the polymer chain with chemical groups possessing strong affinity with the ceramic surface (*i.e.* the "grafting to" technique) or by triggering (co)polymerization of suitable monomers directly from the ceramic surface ("grafting from" approach).[39] Surface-initiated RAFT (reversible addition–fragmentation chain transfer) polymerization is an interesting tool because it leads to the formation of polymer brushes on the ceramic surface with high grafting densities.[40,41] Moreover, the core–shell structure formed by these polymer-decorated particles favours and stabilizes the dispersion of the inorganic nanoparticles in the solvent during the processing route. For example, Ohno *et al.*[42] grafted polyvinylacetate (PVAc) brushes onto silica nanoparticles, then hydrolysed the acetate groups to form polyvinylalcohol (PVA) brushes and showed that the suspension of the resulting nanoparticles in water was greatly enhanced. SI-RAFT was also used by Yang *et al.* to graft polystyrene (PS) brushes[40] and poly (fluorinated acrylates)[43] onto BTO particles. The PS@BTO nanoparticles were compression-moulded to form composites with increased dielectric constant (7.9 times higher) compared to pure PS while BTO with fluorinated shell were used to prepare by solvent casting composites using a poly(vinylidene fluoride-*co*-hexafluoropropene), P(VDF-*co*-HFP), matrix. According to Yang *et al.*,[43] the fluorinated shell increased the dispersion of the nanoparticles in the fluoropolymer matrix, and the resulting composite displayed high energy density and low dielectric loss. The SI-RAFT approach is of particular interest for the fluoropolymers as recent work showed that VDF as well as TrFE polymerisation could be controlled using xanthate agents.[44–47] Indeed, even if those monomers are prone to backwards additions, the RAFT polymerisation using *O*-ethyl-*S*-(1-methoxycarbonyl) ethyldithiocarbonate could afford an acceptable degree of control.

In the present study, piezoelectric composites integrating barium titanate (BTO) nanoparticles incorporated into a P(VDF-*co*-TrFE) copolymer matrix were prepared and their piezoelectric properties investigated. Barium titanate was used as an easily accessible piezoelectric ceramic featuring high piezoelectric coefficient that does not contain harmful components. The piezoelectric P(VDF-*co*-TrFE) copolymer was utilized as polymer matrix because it directly crystallizes in the electroactive crystal phase and it is soluble in a wide panel of organic solvents. An *in situ* polymerization technique was chosen to graft the fluoropolymer chains from BTO particles. A novel chain transfer agent (DOPA-XA) derived from *O*-ethyl-*S*-(1-methoxy-carbonyl) ethyldithiocarbonate, known to successfully control the RAFT polymerization of VDF[48] and TrFE,[45] and integrating a catechol unit was prepared and grafted onto BTO particles. The BTO particles were then decorated with PTrFE or P(VDF-*co*-TrFE) *via* surface-initiated RAFT polymerization leading to hybrid fluoropolymer/BTO particles endowed with a strong ceramic/polymer interface and able to efficiently disperse into a fluoropolymer matrix. The PTrFE@BTO and P(VDF-*co*-TrFE)@BTO nanoparticles were incorporated into a commercial P(VDF-*co*-TrFE) matrix to form composites films by solvent casting. The piezoelectric response of the resulting composites films was then examined and the cohesion of the

BTO/copolymer matrix interface was investigated after mechanical solicitation. To the best of our knowledge, this work reports for the first time, the use of surface-initiated RAFT polymerization of fluoromonomers as coupling method for the preparation of piezoelectric composites.

Materials and methods

Materials

Chemical reagents were purchased from Sigma-Aldrich. *O*-Ethyl-*S*-(1-methoxycarbonyl) ethyldithiocarbonate (CTA-XA) was synthesized according to the method described by Liu *et al.*[49] Methanol was dried by distillation on magnesium. Acetone, petroleum ether, dichloromethane, ethyl acetate, and dimethylcarbonate (DMC) were purchased from Sigma-Aldrich and used as received. $BaTiO_3$ (or BTO) powder (99.95%, electronic grade, average particle size of 200 nm) was purchased from Inframat. P(VDF-*co*-TrFE) (TrFE content = 20% mol, M_n = 200–320 kDa, $Đ$ = 2.6–2.9) was supplied from Arkema.

Methods

Specific surface area measurements. The instrument used was a 3-Flex from Micromeritics. Prior to adsorption measurements, the BTO nanoparticles were degassed for 12 h at 100 °C. The adsorption of the nitrogen was made at 77 K for relative pressure comprised between 0.00057 and 0.9892. The specific surface was measured using Brunauer–Emmett–Teller (BET) theory and the BET equation was applied between the interval of relative pressure [0.05–0.3]. In this interval, the linear regression coefficient is 0.9998371 and the *C* constant was 90.24.

TGA. Thermogravimetric analysis (TGA) experiments were performed with a TGA Q50 apparatus (TA Instruments) from ambient to 700 °C with a heating rate of 10 °C min^{-1}. The sample was placed in an open platinum high temperature pan and the oven was flushed with highly pure nitrogen gas (90 mL min^{-1}, 10%) and oxygen (90%).

DSC. Thermal characterization was achieved on a DSC Q20 (TA Instruments) calibrated using a high purity indium sample. Samples of approximately 10 mg were put into aluminium pans and heated from −80 to 210 °C then cooled from 210 °C to −80 °C and heated again from −80 to 210 °C under nitrogen gas flow. The heating and cooling rates are of 10 °C min^{-1}. The thermograms correspond to the second heating ramp.

SEC. Size-exclusion chromatograms were recorded using a triple-detection 1260 Infinity II Multi-detector from Agilent Technologies with its corresponding Agilent software, dedicated to multidetector GPC calculation. The system used two PL1113-6300 ResiPore 300 × 7.5 mm columns with THF as the eluent with a flow rate of 1 mL min^{-1} and toluene as the flow rate marker. The detector used was a 390-LC PL0390-0601 refractive index detector. The entire SEC-HPLC system was thermostated at 35 °C. PMMA narrow standards were used for calibration (ranging from 500 to 1 500000 g mol^{-1}). Typical sample concentration was 10 mg mL^{-1}.

Nuclear magnetic resonance. Nuclear magnetic resonance (NMR) spectra were recorded on a Bruker AC 400 instrument. Deuterated acetone was used as the solvent in each sample. Coupling constants and chemical shifts are given in hertz (Hz) and parts per million (ppm), respectively. The experimental conditions for recording ^1H and ^{19}F NMR spectra were as follows: flip angle, 90° (or 30°); acquisition time, 4.5 s (or 0.7 s); pulse delay, 2 s (or 2 s); number of scans, 128 (or 512); and pulse width, 5 μs (for ^{19}F NMR). ^{13}C NMR spectra were recorded at 25 °C with a Bruker Avance 300 spectrometer.

X-ray photoelectron spectroscopy. X-ray photoelectron spectroscopy (XPS) analyses were performed on a Kratos Axis Ultra DLD system (Kratos Analytical) using a nonmonochromatic Al Kα X-ray source ($h\nu$ = 1486.6 eV). The emission voltage and the current of this source were set to 12 kV and 3 mA, respectively. The vacuum in the analysing chamber was maintained at 5×10^{-9} mbar or lower during analysis. Survey (0–1320 eV) and high-resolution spectra were recorded at pass energies of 160 and 40 eV, respectively. XPS analyses were performed with a take-off angle of 90° relative to the sample surface. The core-level spectra were referenced with the Ti 2p binding energy at 458.6 eV. Data treatment and peak fitting procedures were performed using Casa XPS software.

Transmission electron microscopy. The transmission electron microscopy (TEM) images were recorded on a Tecnai G2 20 (FEI) operated at 200 kV. Before observations, a suspension of nanoparticles in acetone was deposited on the microscopy grid and let dry for 20 min.

Scanning electron microscopy. The morphology of nanocomposites was investigated by field emission scanning electron microscopy (FE-SEM) using a JEOL JSM-7800F LV (Plateforme de Microscopie Electronique de Lille, University of Lille, France) operated at an acceleration voltage of 5 kV. The micrographs were taken from the surface of unstretched or stretched composites previously coated with carbon (thickness ≈ 20 nm).

Piezoelectric response. Piezoelectric coefficient (d_{33}) was measured on a PiezoMeter System PM300 (Piezotest) at ambient temperature, with a static force of 10 N and a dynamic force of 0.25 N at a frequency of 110 Hz, on composites previously poled under an electric field of 40 MV m^{-1} at T = 110 °C for t = 20 min.

Traction. Dumbbell shaped samples, with dimensions of 12×4 mm^2, were stretched until the fracture with an initial deformation rate of 0.05 s^{-1} at a draw temperatures T_d = 120 °C.

Synthesis

Synthesis of 2-((ethoxycarbonothioyl)thio)propanoic acid (XA-acid). (XA-acid) was synthesized according to the procedure described by Xiang *et al.*[50] An additional vacuum treatment step was necessary to fully remove residual 2-bromopropionic acid (dynamic vacuum, 10 mbar at 80 °C). The product was obtained as a viscous orange oil with a yield of 76%.

^1H NMR ($CDCl_3$, ppm, Fig. S1†): 1.39–1.46 (3H, CH_2CH_3), 1.57–1.65 (3H, $CHCH_3$), 4.30–4.36 (1H, $CHCH_3$) and 4.60–4.65 (2H, CH_2CH_3).

Synthesis of XA-NHS. A suspension of *N*-hydrosuccinimide (NHS, 1.5 eq., 8.9 g, 77 mmol) in dried CH_2Cl_2 was slowly introduced into a solution of acid-XA (1 eq., 10 g, 51.5 mmol) dicyclohexylcarbodiimide (DCC, 1.5 eq., 15.8 g, 77 mmol) and 4-dimethylaminopyridine (DMAP, 1.5 eq., 9.4 g, 77 mmol) in CH_2Cl_2 under N_2 atmosphere at −10 °C. After 12 h of stirring at room temperature, the mixture was washed 3 times with water, the organic phase was dried over $MgSO_4$ and the organic solvent was evaporated under reduced pressure. The product was purified on silica gel column with ethyl acetate/petroleum ether as eluent (1/3).

^{1}H NMR ($CDCl_3$, ppm, Fig. S2†): 1.39–1.46 (3H, CH_2CH_3), 1.68–1.73 (3H, $CHCH_3$), 2.84 (4H, CH_2CH_2) and 4.56–4.72 (2H, CH_2CH_3 and 1H, $CHCH_3$).

Synthesis of *S*-(1-((3,4-dihydroxyphenethyl)amino)-1-oxopropan-2-yl) *O*-ethyl carbonodithioate (DOPA-XA). XA-NHS (4.77 g, 16.4 mmol) and dopamine hydrochloride (4.7 g, 24.6 mmol) were dissolved in dried methanol at room temperature under N_2 atmosphere. After 20 min of stirring, triethylamine (2.75 mL, 19.68 mmol) was added dropwise and the solution was stirred for 24 h in the dark. The solvent was evaporated and the product was redissolved in 150 mL of CH_2Cl_2. The organic phase was washed five times with $NaHCO_3$ solution followed by two washing with H_2O. The organic phase was then dried on $MgSO_4$ and evaporated to produce a viscous and sticky orange oil. The product was purified on silica gel column chromatography using an ethyl acetate/petroleum ether 1 : 1 binary mixture. The product was isolated as a sticky yellow oil with a 28% yield.

^{1}H NMR ($CDCl_3$, ppm): 1.39–1.46 (3H, CH_2CH_3), 1.68–1.73 (3H, $CHCH_3$), 2.6–2.75 (2H, NH–CH_2CH_2), 3.4–3.6 (2H, NH–CH_2CH_2), 4.15–4.35 (1H, $CHCH_3$), 4.56–4.72 (2H, CH_2CH_3) and 6.5–6.9 (3H, Ph).

^{13}C NMR ($CDCl_3$, ppm): 13.7 (CH_2CH_3), 16.3 ($CHCH_3$), 34.6 (NH–CH_2CH_2), 41.2 (NH–CH_2CH_2), 47.9 ($CHCH_3$), 71.0 (CH_2CH_3) and 115.2;11.56;1;120.8 (CH, Ph), 130.6 (CH-CH_2, Ph), 142.9;144.0 (CH-OH, Ph), 171.9 (C═O), 213.1 (C═S).

Grafting of the DOPA-XA onto BTO nanoparticles (Scheme 1). BTO nanoparticles (4 g) were dispersed in a solution of H_2O_2 (30 vol%, 100 mL) by vigorous shaking and repeated cycles in a sonication bath. The mixture was then stirred overnight at 105 °C in a round bottom flask of 250 mL topped with a condenser. The activated BTO-OH particles were then washed by repeated centrifugation cycles with H_2O and then dried in a vacuum oven at 80 °C overnight. The particles (2 g) were re-dispersed in an acetone : water binary mixture (90/10) and 100 mg of DOPA-XA were added, the mixture was stirred for 48 h at room temperature (20 °C). The resulting BTO-XA particles were then washed repeatedly *via* cycles of centrifugation–redispersion in acetone until complete disappearance of the DOPA-XA NMR signal in the supernatant solution. The particles were subjected to TGA to estimate the amount of DOPA-XA grafted on the BTO particles.

Surface initiated RAFT polymerization. SI-RAFT polymerization of vinyl acetate (VAc) was conducted using the following procedure. VAc (3.0 g, 34.8 mmol), CTA-XA (7.3 mg, 3.48×10^{-5} mol), AIBN (2.9 mg, 1.74×10^{-5} mol) and 1 wt% of BTO-DOPA-XA particles were stirred in a 50 mL round bottom flask for 15 min at 0 °C under argon bubbling and then stirred at 70 °C. After 5 h, the reaction was stopped and the particles were washed by cycles of centrifugation–redispersion in acetone until complete disappearance of the ^{1}H NMR polymer signal in the supernatant solution (at least 8 washing cycles). The supernatant solution was evaporated and the free polymer were analyzed by SEC using PMMA standards and NMR. The PVAc@BTO particles were then dried overnight in a vacuum oven at 60 °C and then subjected to TGA to estimate the amount of grafted polymer and the grafting density.

SI-RAFT copolymerization of VDF and TrFE was carried out in thick 8 mL Carius tubes in which a solution of *tert*-amyl peroxy-2-ethylhexanoate (Trigonox® 121, 1.8 mg, 8.03×10^{-6} mol), CTA-XA (5.6 mg, 2.68×10^{-5} mol) and in DMC (3 mL) and 1 mL of a suspension of BTO-DOPA-XA in DMC (70 mg mL^{-1}) was added and then degassed by performing at least three freeze–pump–thaw cycles. The gaseous monomers were introduced into the Carius tube at the liquid nitrogen temperature (TrFE, 0.66 g, 8.03×10^{-3} mol, ΔP = 0.35 bar and VDF, 1.2 g 0.019 mol, ΔP = 0.8 bar) using a custom-made manifold that enables accurate measurement of the amounts of gas (using "pressure drop *vs.* mass of monomer" calibration curves). The tube was then sealed under dynamic vacuum at the liquid nitrogen temperature, before being placed horizon-

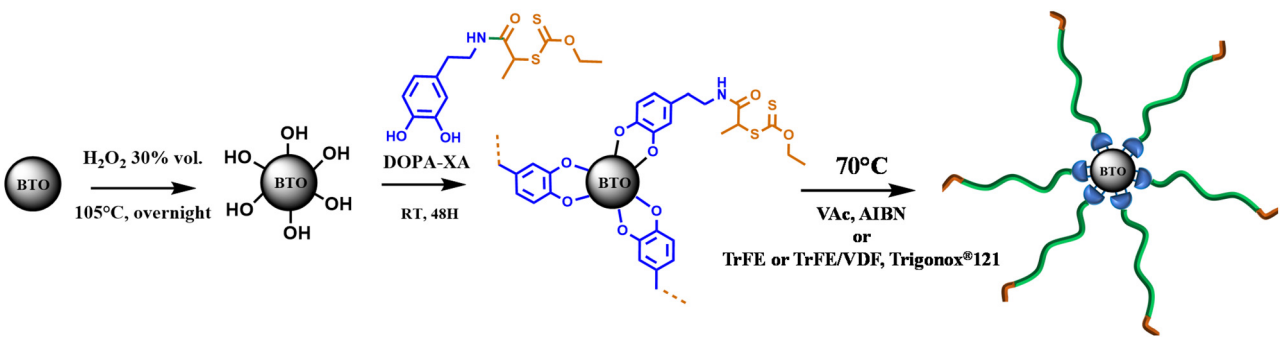

Scheme 1 Schematic representation of the strategy used for the functionalization of BTO nanoparticles with polymers.

tally in a shaking water bath thermostated at 73 °C. The tubes were opened after 16 h of polymerization. The particles were washed by cycles of centrifugation–redispersion in acetone until complete disappearance of the polymer ^{19}F NMR signal in the supernatant solution (at least 5 washing cycles). The supernatant solution was evaporated and the free polymer were analyzed by SEC and ^{1}H and ^{19}F NMR. The P(VDF-*co*-TrFE)@BTO particles were then dried overnight in a vacuum oven at 60 °C and investigated by TGA to estimate the amount of grafted polymer and the grafting density.

SI-RAFT polymerization of TrFE was carried out using the same protocol used for the copolymerization of VDF and TrFE. Briefly, a solution of *tert*-amyl peroxy-2-ethylhexanoate (Trigonox® 121, 1.7 mg, 7.3×10^{-6} mol), CTA-XA (5.1 mg, 2.4×10^{-5} mol) in DMC (3 mL) and 1 mL of a suspension of BTO-DOPA-XA in DMC (70 mg mL^{-1}) was added and then degassed by performing at least three freeze–pump–thaw cycles. The gaseous monomers were introduced into the Carius tube at the liquid nitrogen temperature (TrFE, 2.0 g, 24.3 mmol, $\Delta P = 1.05$ bar).

Composite film preparation. Different BTO/P(VDF-*co*-TrFE) composite films with a unique BTO content of 20 wt% were prepared by solvent-casting. 50 mg of modified BTO particles (PTrFE@BTO and P(VDF-*co*-TrFE)@BTO) were dispersed into 2 mL of acetone and the resulting dispersion was placed in a sonicating bath for 30 min. 200 mg of P(VDF-*co*-TrFE) was solubilized in 2 mL of acetone and this solution was added to the BTO particles suspension. The reaction mixture was placed in a sonicating bath. The solution was then drop-casted in a silicone mould (6 cm of diameter). The mould was left for 24 h in a fume hood then placed in a vacuum oven for 4 h at 80 °C to remove any trace of remaining solvent. Finally, the films were compression moulded at 210 °C for 5 min under a pressure of 50 bars and then cooled down to room temperature. The resulting composites were finally annealed at 135 °C for 2 h in an oven. The annealing temperature was chosen between the Curie temperature and the melting temperature of the polymer matrix according to the work of Bargain *et al.*[51] to improve the ferroelectric crystal phase of the P(VDF-*co*-TrFE) copolymer. The resulting composite films had an average thickness of around 55 ± 5 μm. For comparison, a composite made with unmodified BTO was prepared following the same procedure. The composites are denoted BTO/CP, PTrFE@BTO/CP and CP@BTO/CP for copolymer matrix composites with BTO, PTrFE@BTO and P(VDF-*co*-TrFE)@BTO respectively.

Results and discussion

The strategy adopted to functionalize the barium titanate nanoparticles (BTO, diameter of 200 nm) is described in Scheme 1. The ceramic surface was pre-treated with hydrogen peroxide (35vol%) to increase the concentration of hydroxyl groups at the surface of the nanoparticles. Then, a new RAFT agent integrating a catechol fragment and a xanthate moiety (DOPA-XA) is grafted on the activated particles (BTO-OH) to obtain functionalized nanoparticles featuring xanthate moieties (BTO-XA). The BTO-XA surfaces were then used to mediate the SI-RAFT polymerization of TrFE and VDF from BTO nanoparticles surface.

Synthesis of the DOPA-XA

The RAFT agent DOPA-XA featuring a catechol group capable of binding onto BTO nanoparticles surface was prepared in two steps from 2-((ethoxycarbonothioyl)thio)propanoic acid and dopamine hydrochloride (Scheme 2). A particular attention was paid to introduce the catechol moiety on the R-group (re-initiating part) of the chain transfer agent to induce an efficient "grafting from" process from the BTO particles.[52]

DOPA-XA was conveniently prepared from the coupling reaction of the *N*-hydroxysuccinimide activated ester of 2-((ethoxycarbonothioyl)thio)propanoic acid[50] and commercially available dopamine hydrochloride. This synthesis was adapted from a previously reported procedure dealing with the preparation of a catechol-functionalised trithiocarbonate RAFT agent.[53] The structure of DOPA-XA was confirmed by ^{1}H NMR and ^{13}C NMR (see ESI Fig. S3 and S4†). The ^{1}H NMR spectrum of DOPA-XA (Fig. 1) revealed the presence of the characteristic

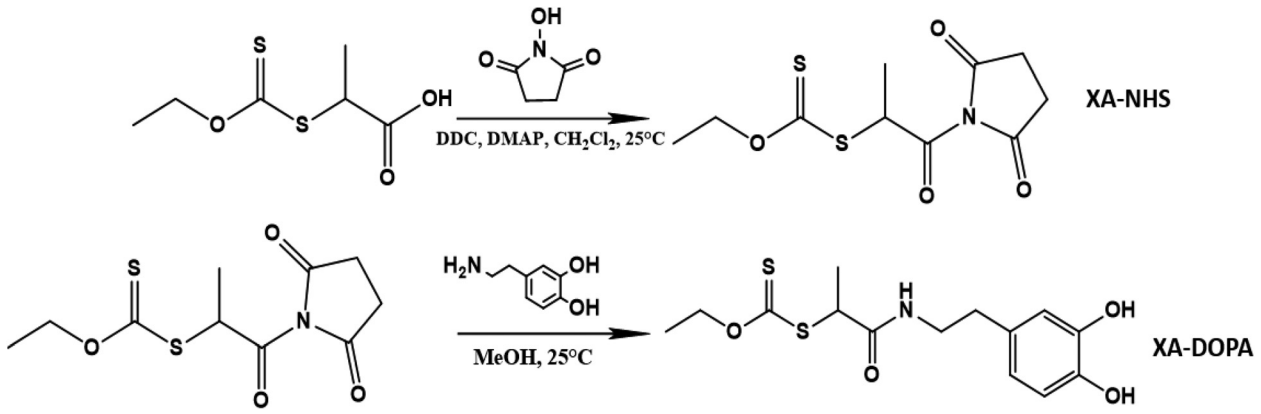

Scheme 2 Synthesis of DOPA-XA.

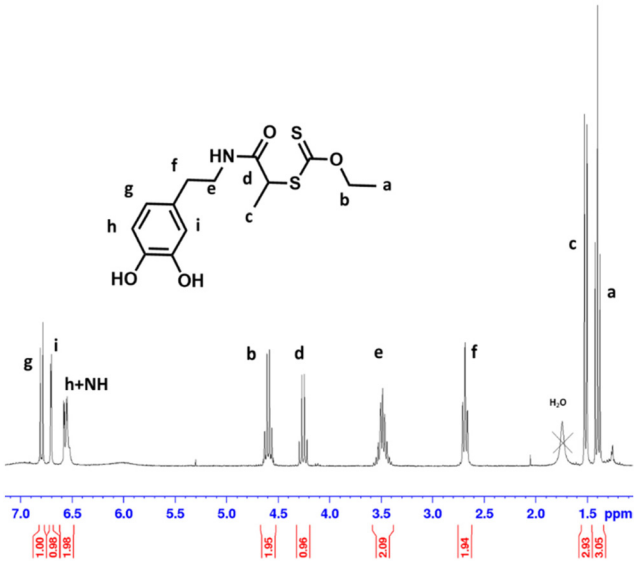

Fig. 1 ^{1}H NMR spectrum of DOPA-XA recorded in $CDCl_3$ at 25 °C.

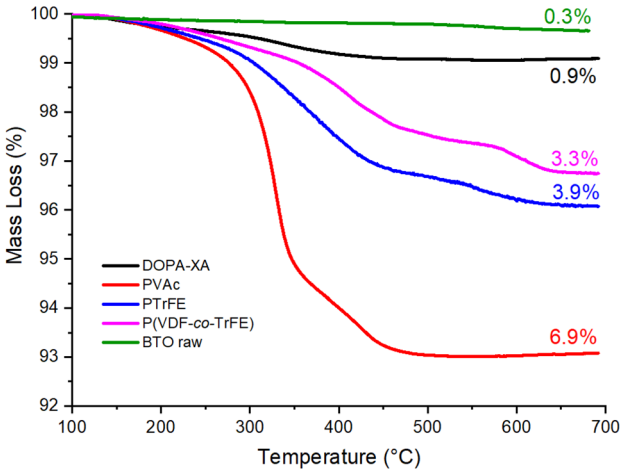

Fig. 2 TGA thermograms of raw BTO (green line) and BTO grafted with DOPA-XA (black line), with P(VDF-*co*-TrFE) (magenta line), with PTrFE (blue line) or with PVAc (red line). The H_2O_2 treatment had no impact on the TGA thermogram of the BTO particles.

signals of the catechol unit (6.5 to 7 ppm) and of the xanthate moiety at 1.3 and 4.6 ppm. Furthermore, the ^{13}C spectrum (Fig. S1†) clearly displayed chemical shifts at 171.9 and 213.0 ppm ascribed to the amide carbonyl group and the thiocarbonyl fragment, respectively. DOPA-XA was not isolated in high yields due to significant loss during the flash chromatography purification process.

Grafting of DOPA-XA onto BTO nanoparticles

BTO nanoparticles with an average diameter of 200 nm were first activated to increase the density of hydroxyl groups on the BTO surface and allow the binding of a higher number of DOPA-XA molecules.[54] Indeed, catechol groups display different interactions with surface hydroxyl groups including coordination[55] (mostly with metallic materials), covalent bonding,[56] and hydrogen bonding,[57] the latter occurring with very hydrophilic surfaces. The activation procedure employed a solution of 35 vol% of hydrogen peroxide to generate hydroxyl groups at the surface of the BTO according to the work of Yang *et al.*[40] and provided hydroxylated BTO surface labelled BTO-OH nanoparticles. DOPA-XA was then immobilized onto the surface of these BTO-OH nanoparticles as follows. BTO-OH particles were dispersed in a solution of DOPA-XA (10^{-2} M) solubilized in a protic acetone/water (90/10) binary mixture to favour the interactions between the catechol and the hydroxyl groups on the BTO-OH NPs surface.

The grafting of the DOPA-XA onto the BTO NPs was investigated by TGA measurements (Fig. 2). The thermogram of the pristine BTO (raw BTO) particles showed a small mass loss of around 0.3% probably due to solvent or species poorly bonded on the BTO surface whereas the BTO-XA showed a mass loss of 0.9% in the 150 to 450 °C range corresponding to the thermal degradation of the DOPA-XA unit as depicted in Fig. S5.† The measurements of this mass loss and of the specific surface area of the raw BTO NPs by BET (*ca.* 4.5 m^2 g^{-1}) allowed the estimation of the DOPA-XA grafting density at 3.7 molecules per nm^2 (see eqn (S1)†). This value is higher than the grafting density reported by Khani *et al.*[58] (0.16 molecules per nm^2), who modified amino-functionalized silica particles with a NHS-activated dithiobenzoate CTA but is in good agreement with previous studies by Ohno *et al.*[42] dealing with the direct immobilisation of a silane-modified xanthate onto silica nanoparticles.

Further evidence of the grafting of DOPA-XA on the BTO NPs was obtained from XPS measurements. As depicted in Fig. 3, the XPS survey of the DOPA-XA-grafted BTO surface displayed the characteristic chemical elements of the DOPA-XA moiety. Indeed, a component at 398.4 eV was observed in the N 1s core level spectrum while two components at 151.6 and 162.7 eV were detected in the S 2p core level spectra and are attributed to nitrogen and sulfur chemical elements of DOPA-XA thus demonstrating the presence of DOPA-XA on the BTO surface. In addition, a S/N ratio of 2.38 was calculated from the XPS semi-quantitative analysis of the functionalized BTO in accordance with the theoretical ratio (S/N theoretical ratio = 2) from the DOPA-XA structure.

Surface-initiated RAFT polymerization from BTO

The surface-initiated RAFT polymerization was first conducted with vinyl acetate (VAc) as a test monomer to establish the suitability of the DOPA-XA@BTO NPs to mediate RAFT polymerization since VAc belongs to the Less Activated Monomers (LAMs) like VDF or TrFE and is thus controlled by xanthate RAFT agents.

The conditions were adapted from the work of Ohno *et al.*[42] who synthesized PVAc-decorated silica particles using SI-RAFT polymerization. The polymerization was carried out using *O*-ethyl-*S*-(1-methoxycarbonyl) ethyldithiocarbonate (CTA-XA) as a free xanthate agent containing the same Z group as the

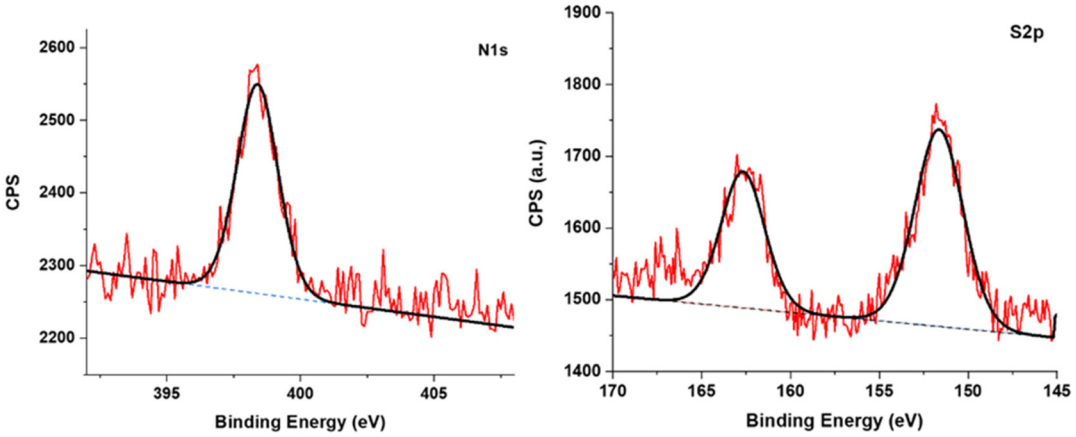

Fig. 3 XPS spectra of the BTO nanoparticles functionalized with DOPA-XA showing the N 1s (left) and S 2p (right) core level regions.

grafted DOPA-XA and known to control the RAFT polymerization of VDF[48] and TrFE.[45] According to Ohno *et al.*, the role of this free CTA-XA in solution is to promote the exchange reactions between the free and grafted macroradicals thus affording a better control over the polymerisation. In addition, the same authors demonstrated that the free macroradicals have the same propagation rate as the grafted ones, making them remarkable tools to monitor the polymerisation.[52] The reactions were conducted using 1 wt% of BTO-DOPA-XA nanoparticles without solvent. The small amount of CTA fixed on the BTO particles (4.7 mg of DOPA-XA for 1 g of BTO) was neglected as it represents only 5 mol% of the total amount of the free CTA used. The high[CTA-XA] : [VAc] (1 : 1000) molar ratio was chosen to obtain high molar mass polymer brushes.

After the polymerization, the free PVAc was separated from the reaction mixture by centrifugation and the conversion was analysed by NMR and the molar masses were analysed by SEC (Table 1) while the grafted NPs were analysed by TGA and TEM. ^{1}H NMR and SEC analyses performed on the free PVAc polymer reveal a M_n of 32 000 g mol^{-1} and a dispersity of 1.53 (entry 1, Table 1). This number average molar mass value may seem low compared to the theoretical 81 000 g mol^{-1} but could be explained by the combined effect of the PMMA calibration of the SEC instrument and the relatively high dispersity. This relatively broad molar mass distribution was expected, since VAc is prone to chain inversions which lead to a slowdown of the RAFT equilibrium and some loss of the control of the polymerization.[59] The TEM images of the PVAc@BTO nanoparticles (Fig. 5b) clearly showed the PVAc polymer layer at the surface of the BTO nanoparticles with a thickness of 7.2 ± 1.5 nm. The grafting of PVAc was further demonstrated by TGA experiment which showed a mass loss of 6.9% for the PVAc@BTO NPs. Considering the average diameter of the BTO NPS, the M_n of the PVAc estimated by SEC (32 000 g mol^{-1}) and the mass loss measured by TGA, a grafting density of 0.30 chains per nm^2 was calculated from eqn (S1)†. This grafting density is approximately ten times lower than that of DOPA-XA in agreement with previous reports dealing with surface initiated polymerization.[60,42,52]

SI-RAFT polymerization was then conducted with fluoromonomers (entries 2 (TrFE) and 3 (VDF + TrFE) in Table 1). The polymerization conditions were chosen in agreement with the work of Guerre *et al.*[47,48] and Bouad *et al.*[44,45] The polymerization were conducted in dimethycarbonate (DMC) as this solvent has been shown to provide high polymerization rates and to be relatively less prone to transfer with the fluorinated macroradicals than other solvents.[61] As for the polymerization of VAc, a high [CTA-XA] : [Monomer] ratio was chosen (1 : 1000) to obtain high molar mass polymer brushes. The [VDF] : [TrFE] ratio was chosen at 7 : 3, close to the azeotropic blend composition, to reduce drastically the compositionnal drift which would occur otherwise due to the different reactivity ratios of VDF and TrFE ($r_{VDF-TrFE}$ = 0.77 ± 0.04 and $r_{TrFE-VDF}$ = 0.32 ± 0.02).[62,63] As the reaction was carried out in a sealed Carius

Table 1 SI-RAFT polymerization from BTO NPs

Entry	Reaction time (h)	Monomer	[M] : [CTA] : [I] [d]	Conversion (%)	M_{nGPC} (g mol^{-1})	$Đ$	Mass loss[e] (%)	Graft density (chains per nm^2)
1[a]	5	VAc	1000 : 1 : 0.5	94	32 000	1.53	6.9	0.30
2[b]	16	TrFE	1000 : 1 : 0.3	––	23 500	1.52	3.9	0.21
3[b]	16	VDF & TrFE[c]	1000 : 1 : 0.3	––	12 400	1.9	3.3	0.33

[a] Polymerization conducted in bulk at 70 °C during 5 h. I = AIBN. [b] Polymerizations conducted in dimethylcarbonate, [M] = 6 mol L^{-1}, 73 °C for 16 h. I = *tert*-amyl peroxy-2-ethylhexanoate. [c] [VDF] : [TrFE] = 7 : 3. [d] Particle concentration was around 1%wt, the amount of XA moities grafted on the particules was negleted. [e] Mass loss recorded by TGA on polymer-grafted -nanoparticles.

tube, the monitoring of the reaction was impossible. At the end of the polymerization, the free polymer chains were separated from the decorated particles and subjected to ^{19}F NMR and SEC measurements. As expected, the free PTrFE chains had high molar masses and acceptable dispersity (M_n (SEC) = 23 500 g mol^{-1} and $Đ$ = 1.5, entry 2 in Table 1). TrFE is even more prone to chain inversions or transfer reactions than VAc or VDF which lead to faster slowdown of the RAFT equilibrium and higher fraction of dead chains responsible for the significant increase in dispersity observed.[44,45] This was confirmed by the ^{19}F NMR investigations of the free PTrFE that showed an important loss of the chain end functionality as only 50% of these PTrFE chains were terminated by a xanthate moiety (-CFH-XA at −171 and −175 ppm, Fig. 4) at the end of the polymerization.[44] The chains-ends resulting from irreversible transfer[44] (*i.e.* terminated by a –CF_2H group at −132 ppm or a –CFH_2 group at −244.6 ppm, Fig. 4) constituted the other half of the PTrFE chains. The free P(VDF-*co*-TrFE) chains resulting from the copolymerization of VDF and TrFE mediated by the free RAFT agent had lower molar mass (13 500 g mol^{-1}) and higher dispersity (1.9) than the free PTrFE. Lack of knowledge on the ^{19}F NMR signals of the chains ends of P(VDF-*co*-TrFE) copolymers made by RAFT polymerization prevents the estimation of the chain-end functionality. However, the relatively high dispersity observed is likely caused by the chain inversion and irreversible transfer phenomena that are known to occur for both RAFT homopolymerization of VDF and TrFE.[45,47]

After the polymerization and several purification steps (centrifugation–redispersion), the particles were examined by TEM (Fig. 5). The TEM analyses revealed homogeneous polymer layers on the BTO nanoparticles with thicknesses of 2.9 ± 0.9 nm for the PTrFE@BTO (Fig. 5c) and 3.0 ± 1.2 nm for the P(VDF-*co*-TrFE)@BTO (Fig. 5d).

TGA analyses (Fig. 2) were performed to further demonstrate the grafting of the fluoropolymer layer onto the BTO nanoparticles. The PTrFE@BTO and P(VDF-*co*-TrFE)@BTO NPs

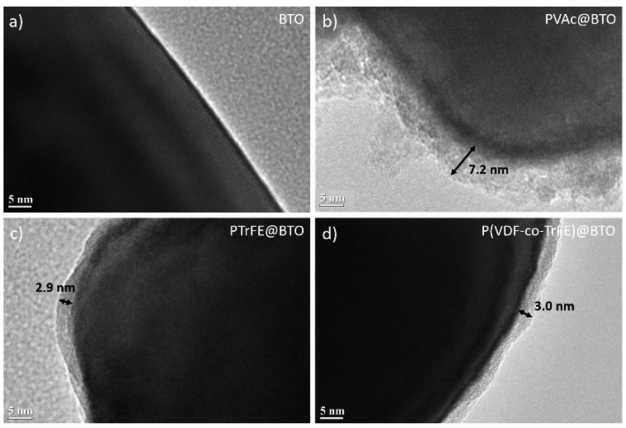

Fig. 5 TEM images of (a) raw BTO, (b) PVAc@BTO, (c) PTrFE@BTO and (d) P(VDF-*co*-TrFE)@BTO.

thermograms showed mass losses of 3.9% and 3.3% respectively, leading to estimated grafting densities of 0.2 and 0.3 chains per nm^2 following the calculations described in eqn (S1)†. These values are in good agreement with previous results found for the SI-RAFT of VAc.[42]

Finally, the presence of a fluoropolymer layer on the BTO surface was investigated by XPS experiments. The XPS survey spectra of the raw and fluoropolymer-grafted BTO surfaces are presented Fig. 6. Interestingly, a decrease of the Ba 3d and Ti 2p signals from BTO was observed on PTrFE@BTO and P(VDF-*co*-TrFE)@BTO survey spectra (see Table S1†) compared to the raw BTO survey spectra, suggesting the presence of a grafted layer on the surface. Moreover, the XPS surveys of the functionalized particles clearly show the presence of fluorine in the grafted film as a F 1s component at 686.9 eV was observed in both cases thus confirming the presence of fluoropolymer on the BTO surface.

The incorporation of nanoparticles bearing polymer brushes in a polymer matrix to promote interfacial adhesion

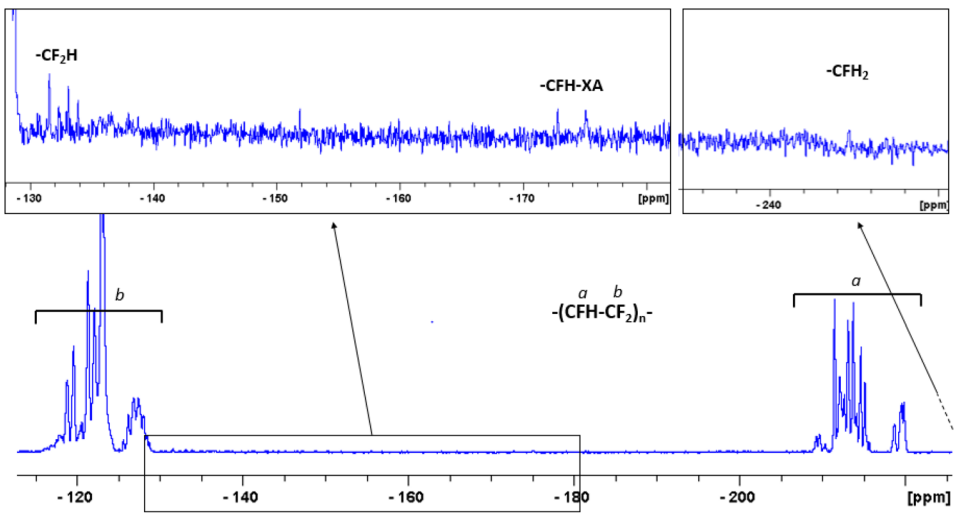

Fig. 4 ^{19}F NMR spectrum of the free PTrFE chains recorded in $CDCl_3$. The complexity of the backbone signal is due to tacticity and chain defects.[44]

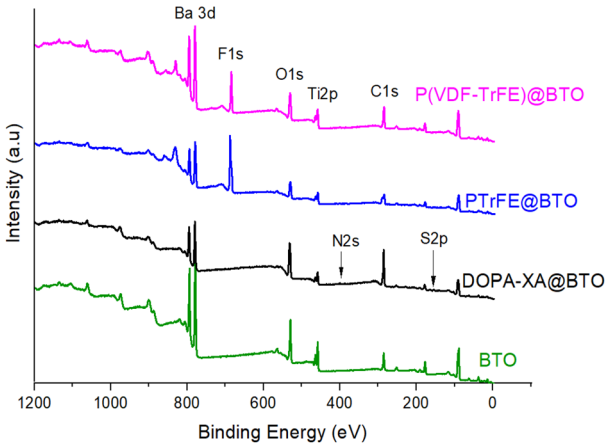

Fig. 6 XPS survey spectra of raw BTO (green) and P(VDF-*co*-TrFE)@BTO (magenta), PTrFE@BTO (blue), DOPA-XA@BTO (black). Elaboration and piezoelectric properties of BTO based composites.

as already been described in the literature[64,65] in particular in dielectric composites.[66] In this work, the same strategy was used to compatibilize the piezoelectric ceramic and the fluorocopolymer.

BTO, PTrFE@BTO and P(VDF-*co*-TrFE)@BTO particles were separately incorporated into a P(VDF-*co*-TrFE) matrix to prepare three different piezoelectric composites labelled BTO/CP, PTrFE@BTO/CP and CP@BTO/CP respectively. As expected, dispersing the PTrFE@BTO and P(VDF-*co*-TrFE)@BTO NPs in acetone was easier than dispersing the non-modified BTO. This observation is likely due to the presence of the polymer brushes grafted on the BTO particles which greatly stabilizes the dispersion in acetone as PTrFE and P(VDF-*co*-TrFE) show good solubilities in this solvent.

As the quality of the dispersion of BTO nanoparticles in the polymer matrix play an essential role on the nanocomposite physical properties, SEM images of the nanocomposites surface were recorded. As depicted in Fig. 7 the BTO/CP composite made from pristine BTO particles showed large domains of nanoparticles aggregation at a few micrometres scale with ceramic rich and polymer-rich areas. On the contrary, in the PTrFE@BTO/CP and CP@BTO/CP composites, the distribution of PTrFE@BTO and P(VDF-*co*-TrFE)@BTO nanoparticles appeared fairly homogeneous.

The DSC thermograms of the composites made with non-modified BTO, PTrFE@BTO and P(VDF-*co*-TrFE)@BTO presented in Fig. S6† did not show any difference in the Curie or melting temperatures and of the melt enthalpy. This indicates that the addition of modified BTO particles has no impact on the transition temperatures and on the crystalline properties of the polymer matrix.

In order to assess the piezoelectric responses, the three composite films were poled at 40 MV m^{-1} (*i.e.* at an electrical field lower than the breakdown strength) to allow the comparison of the piezoelectric coefficient (d_{33}) with the same poling conditions. The measured d_{33} coefficient was quasi identical for the three composites with values of −9.2, −8.9 and −8.8 pC N^{-1} for BTO/CP, PTrFE@BTO/CP and CP@BTO/CP respectively. These results suggesting that the quality of the BTO dispersion did not have much impact on the piezoelectric response of the composites can actually be explained by the "under-solicitation" of the BTO nanoparticles during the poling step. Indeed, since the BTO particles have a much higher relative permittivity than the copolymer matrix, the effective electric field in the ceramic is greatly lower than the externally applied field.[67]

Finally, in order to probe the efficiency of the interphase, the composites were mechanically solicited by uniaxial stretching at 120 °C with an initial strain rate of 0.05 s^{-1}. Fracture areas were then observed by SEM (Fig. 8).

At different microscopic scales, the SEM image of the BTO/CP composite showed a heterogeneous deformation with some stretched and unstretched areas related to the presence of BTO aggregates. In contrast, for the PTrFE@BTO/CP and CP@BTO/CP composites, fibrillar structures characteristic of the stretched copolymer[68] with a fairly homogeneous BTO distribution were visible. At higher magnification, a significant number of cavities induced by the mechanical solicitation were visible close to the BTO nanoparticles in the BTO/CP composites (white arrows in Fig. 8d), while the grafting of the fluoropolymer layer onto the BTO nanoparticles was efficient enough to maintain a good interfacial adhesion with the copolymer matrix. If this strong interfacial cohesion was the desired result, it is somewhat surprising. Indeed, the relatively

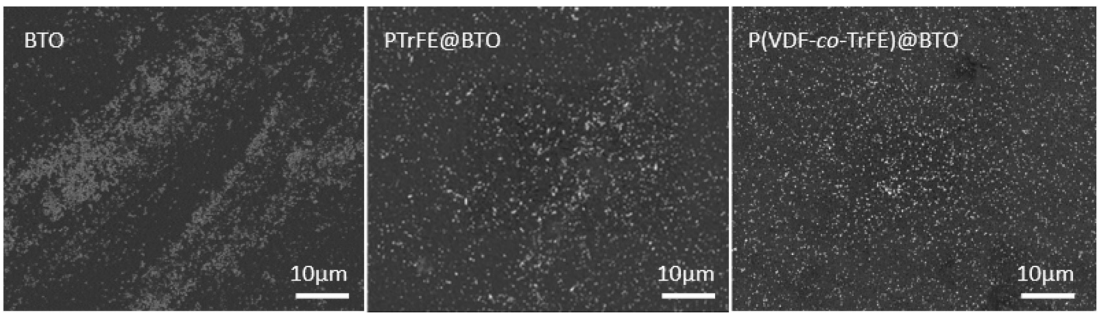

Fig. 7 SEM images of BTO, P(TrFE) @BTO and P(VDF-co-TrFE)@BTO nanoparticles embedded in a P(VDF-co-TrFE) matrix. The filler content was around 20 wt%.

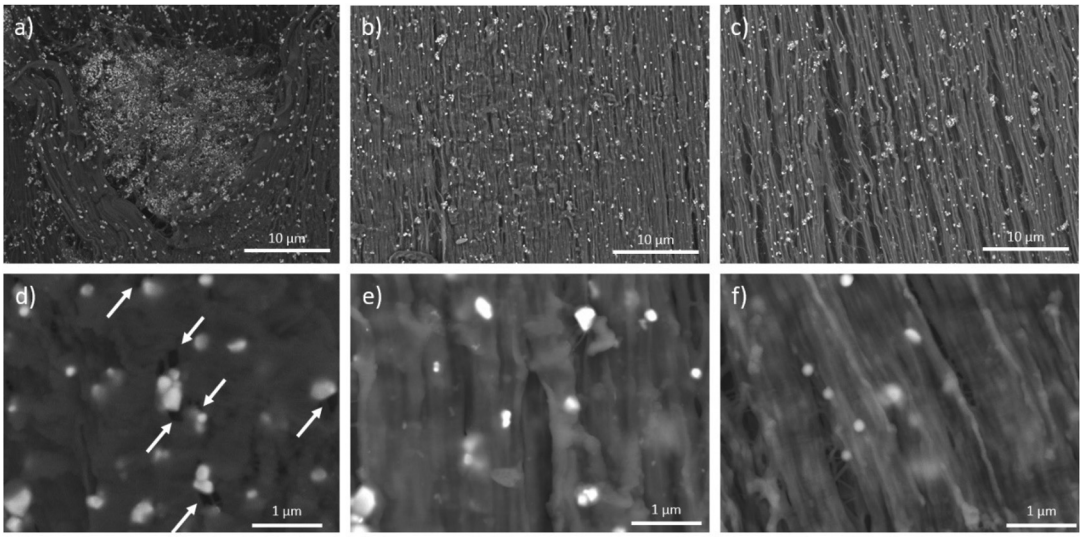

Fig. 8 SEM images of stretched (a)–(d) BTO/CP, (b)–(e) PTrFE@BTO/CP and (c)–(f) CP@BTO/CP. Draw axis is vertical.

high grafting density of the fluoropolymer brushes (around 0.2–0.3 chains per nm^2) indicates that they are in the concentrated polymer brush (CPB) regime which has been shown to hinder chain entanglement *via* size exclusion effect.[69–71] This somewhat surprising result may be caused by the relatively high dispersity of the grafted polymers (1.5–1.9) which may prevent the size exclusion effect usually observed with polymer brushes featuring narrower molar mass distributions.

This study therefore shows the efficiency of using BTO piezoelectric nanoparticle grafted with a fluoropolymer layer such as PTrFE or P(VDF-*co*-TrFE) to obtain a cohesive interface with a P(VDF-*co*-TrFE) piezoelectric fluoropolymer matrix.

Conclusion

This work reports the preparation of Barium Titanate (BTO) – P(VDF-*co*-TrFE) piezoelectric composite using BTO nanoparticles decorated with fluoropolymers. A new xanthate chain transfer RAFT agent possessing a catechol unit was designed and grafted onto the surface of BTO nanoparticles with high grafting densities (>2 molecules per nm^2). This grafted RAFT agent was used to mediate the SI-RAFT polymerization of vinyl acetate, and the copolymerization of trifluoroethylene and vinylidene fluoride from BTO nanoparticles surface with controlled molar mass and acceptably low molar mass distributions for these polymers. The fluoropolymer-functionalized BTO nanoparticles were incorporated into a P(VDF-*co*-TrFE) matrix to prepare piezoelectric composites. Interestingly, the functionalization of BTO nanoparticles by the fluoropolymers afforded better dispersions of the decorated nanoparticles in the fluoropolymer matrix. Moreover, under mechanical solicitation the interface between the functionalized BTO and the polymer matrix was shown to be more cohesive. The use of this functionalization strategy could greatly reduce the problems of compatibility between the polymer and the ceramic phases in piezoelectric composites paving the way for promising applications in piezoelectric devices. This work is aimed at getting better insights of ceramic/polymer interface in piezoelectric composites.

Conflicts of interest

There are no conflicts to declare.

Acknowledgements

This work was partly supported by the Japan Society for the Promotion of Science (JSPS) Summer program fellowship and the Kyoto University, Institute for Chemical Research International Joint Research programme 2019 (iJURC) granted to VB and VL respectively. This work was partly supported by the French National Research Agency (NanoPiC grant, ANR-16-CE08-0025). K. O. also acknowledges the funding from the Japan Society for the Promotion of Science (JSPS) KAKENHI Grants (No. 21H02000). The authors thank Arkema (Pierre-Bénite, France) for providing TrFE, VDF and P(VDF-*co*-TrFE). This work was carried out on the Electron Microscopy facility of the Advanced Characterization Platform of the Chevreul Institute. Technical assistance from Dr Alexandre Fadel in scanning electron microscopy experiments is gratefully acknowledged.

References

1 J. Curie and P. Curie, *Bull. Soc. Fr. Mineral.*, 1880, **3**, 90–93.
2 W. Wersing, G. Zorn, K. Lubitz and J. Mohaupt, *Jpn. J. Appl. Phys.*, 1985, **24**, 724–726.
3 M. Acosta, N. Novak, V. Rojas, S. Patel, R. Vaish, J. Koruza, G. A. Rossetti and J. Rödel, *Appl. Phys. Rev.*, 2017, **4**, 041305.

4 A. Hamieh, F. Ponchel, S. Barrau and D. Remiens, *Ferroelectrics*, 2020, **556**, 79–86.
5 W. Hooker, NASA Langley Tech. Rep. Serv.
6 A. Safari, *J. Phys. III*, 1994, **4**, 1129–1149.
7 B. Malič, D. Kuščer, M. Vrabelj and J. Koruza, in *Magnetic, Ferroelectric, and Multiferroic Metal Oxides*, Elsevier, 2018, pp. 95–120.
8 C. Ribeiro, C. M. Costa, P. Martins, V. Correia and S. Lanceros-Mendez, in *Reference Module in Materials Science and Materials Engineering*, Elsevier, 2018, pp. 1–11.
9 M. P. Wenger, P. L. Almeida, P. Blanas, R. J. Shuford and D. K. Das-Gupta, *Polym. Eng. Sci.*, 1999, **39**, 483–492.
10 T. Kitayama and S. Sugawara, Study Comm. Electron. Circuit Components Mater.
11 H. Kawai, *Jpn. J. Appl. Phys.*, 1969, **8**, 975–976.
12 R. G. Kepler and R. A. Anderson, *Adv. Phys.*, 2006, **41**, 1–57.
13 N. Jia, Q. He, J. Sun, G. Xia and R. Song, *Polym. Test.*, 2017, **57**, 302–306.
14 P. Martins, A. C. Lopes and S. Lanceros-Mendez, *Prog. Polym. Sci.*, 2014, **39**, 683–706.
15 A. Gebrekrstos, G. Madras and S. Bose, *Cryst. Growth Des.*, 2019, **19**, 5441–5456.
16 J. Defebvin, S. Barrau, G. Stoclet, C. Rochas and J. M. Lefebvre, *Polymer*, 2016, **84**, 148–157.
17 R. Hasegawa, Y. Takahashi, Y. Chatani and H. Tadokoro, *Polym. J.*, 1972, **3**, 600–610.
18 M. Kobayashi, K. Tashiro and H. Tadokoro, *Macromolecules*, 1975, **8**, 158–171.
19 S. Weinhold, M. H. Litt and J. B. Lando, *Macromolecules*, 1980, **13**, 1178–1183.
20 A. J. Lovinger, *Macromolecules*, 1982, **15**, 40–44.
21 Y. Tajitsu, in *Soft Actuators*, Springer Japan, Tokyo, 2014, vol. 9784431547, pp. 203–215.
22 B. Ploss, B. Ploss, F. G. Shin, H. L. W. Chan and C. L. Choy, *Appl. Phys. Lett.*, 2000, **76**, 2776–2778.
23 S. T. Lau, K. Li and H. L. W. Chan, *Ferroelectrics*, 2004, **304**, 19–22.
24 L. Zhu and Q. Wang, *Macromolecules*, 2012, **45**, 2937–2954.
25 J. Chon, S. Ye, K. J. Cha, S. C. Lee, Y. S. Koo, J. H. Jung and Y. K. Kwon, *Chem. Mater.*, 2010, **22**, 5445–5452.
26 F. J. Baltá Calleja, A. González Arche, T. A. Ezquerra, C. Santa Cruz, F. Batallán, B. Frick and E. López Cabarcos, *Adv. Polym. Sci.*, 1993, **108**, 3–27.
27 M. F. Lin, V. K. Thakur, E. J. Tan and P. S. Lee, *RSC Adv.*, 2011, **1**, 576–578.
28 K. Prabakaran, S. Mohanty and S. K. Nayak, *J. Mater. Sci.: Mater. Electron.*, 2014, **25**, 4590–4602.
29 N. Jia, Q. Xing, G. Xia, J. Sun, R. Song and W. Huang, *Mater. Lett.*, 2015, **139**, 212–215.
30 S. Dalle Vacche, F. Oliveira, Y. Leterrier, V. Michaud, D. Damjanovic and J. A. E. Månson, *J. Mater. Sci.*, 2012, **47**, 4763–4774.
31 S. D. Vacche, D. Damjanovic, V. Michaud and Y. Leterrier, *Materials*, 2020, **13**, 1–15.
32 Y. Ai, J. Nie, G. Wu and D. Yang, *J. Appl. Polym. Sci.*, 2014, **131**, 41102.
33 A. Mayeen, M. S. Kala, S. Sunija, D. Rouxel, R. N. Bhowmik, S. Thomas and N. Kalarikkal, *J. Alloys Compd.*, 2020, **837**, 155492.
34 J. Defebvin, S. Barrau, J. Lyskawa, P. Woisel and J. M. Lefebvre, *Compos. Sci. Technol.*, 2017, **147**, 16–21.
35 Y. Song, Y. Shen, H. Liu, Y. Lin, M. Li and C. W. Nan, *J. Mater. Chem.*, 2012, **22**, 16491–16498.
36 Y. Zhang, J. Gao, H. Li, E. Wang, J. Zhang and L. Zhang, *J. Mater. Sci.: Mater. Electron.*, 2016, **27**, 11733–11738.
37 Y. Niu, Y. Bai, K. Yu, Y. Wang, F. Xiang and H. Wang, *ACS Appl. Mater. Interfaces*, 2015, **7**, 24168–24176.
38 Y. Niu, K. Yu, Y. Bai, F. Xiang and H. Wang, *RSC Adv.*, 2015, **5**, 64596–64603.
39 Y. Zhao and S. Perrier, *Adv. Polym. Sci.*, 2016, **270**, 77–106.
40 K. Yang, X. Huang, L. Xie, C. Wu, P. Jiang and T. Tanaka, *Macromol. Rapid Commun.*, 2012, **33**, 1921–1926.
41 S. Perrier, *Macromolecules*, 2017, **50**, 7433–7447.
42 K. Ohno, Y. Yahata, M. Sakaue and V. Ladmiral, *Chem. – Eur. J.*, 2019, **25**, 2059–2068.
43 K. Yang, X. Huang, Y. Huang, L. Xie and P. Jiang, *Chem. Mater.*, 2013, **25**, 2327–2338.
44 V. Bouad, M. Guerre, S. Zeliouche, B. Améduri, C. Totée, G. Silly, R. Poli and V. Ladmiral, *Polym. Chem.*, 2021, **12**, 2293–2304.
45 V. Bouad, M. Guerre, C. Totée, G. Silly, O. Gimello, B. Améduri, J.-F. Tahon, R. Poli, S. Barrau and V. Ladmiral, *Polym. Chem.*, 2021, **12**, 2271–2281.
46 M. Guerre, G. Lopez, T. Soulestin, C. Totée, B. Améduri, G. Silly and V. Ladmiral, *Macromol. Chem. Phys.*, 2016, **217**, 2275–2285.
47 M. Guerre, S. M. W. Rahaman, B. Améduri, R. Poli and V. Ladmiral, *Macromolecules*, 2016, **49**, 5386–5396.
48 M. Guerre, B. Campagne, O. Gimello, K. Parra, B. Ameduri and V. Ladmiral, *Macromolecules*, 2015, **48**, 7810–7822.
49 X. Liu, O. Coutelier, S. Harrisson, T. Tassaing, J. D. Marty and M. Destarac, *ACS Macro Lett.*, 2015, **4**, 89–93.
50 Y. Xiang, L. Li and S. Zheng, *Polymer*, 2018, **138**, 113–123.
51 F. Bargain, P. Panine, F. Domingues Dos Santos and S. Tencé-Girault, *Polymer*, 2016, **105**, 144–156.
52 K. Ohno, T. Akashi, Y. Huang and Y. Tsujii, *Macromolecules*, 2010, **43**, 8805–8812.
53 C. Zobrist, J. Sobocinski, J. Lyskawa, D. Fournier, V. Miri, M. Traisnel, M. Jimenez and P. Woisel, *Macromolecules*, 2011, **44**, 5883–5892.
54 J. Saiz-Poseu, J. Mancebo-Aracil, F. Nador, F. Busqué and D. Ruiz-Molina, *Angew. Chem., Int. Ed.*, 2019, **58**, 696–714.
55 W. Laure, D. Fournier, P. Woisel and J. Lyskawa, *Langmuir*, 2017, **33**, 3434–3443.
56 H. Lee, N. F. Scherer and P. B. Messersmith, *Proc. Natl. Acad. Sci. U. S. A.*, 2006, **103**, 12999–13003.
57 Q. Ye, F. Zhou and W. Liu, *Chem. Soc. Rev.*, 2011, **40**, 4244.
58 M. M. Khani, D. Woo, E. L. Mumpower and B. C. Benicewicz, *Polymer*, 2017, **109**, 339–348.

59 M. Guerre, S. M. Wahidur Rahaman, B. Améduri, R. Poli and V. Ladmiral, *Polym. Chem.*, 2016, **7**, 6918–6933.
60 K. Ohno, T. Morinaga, K. Koh, Y. Tsujii and T. Fukuda, *Macromolecules*, 2005, **38**, 2137–2142.
61 A. D. Asandei, O. I. Adebolu and C. P. Simpson, *J. Am. Chem. Soc.*, 2012, **134**, 6080–6083.
62 T. Soulestin, P. Marcelino Dos Santos Filho, V. Ladmiral, C. Totée, G. Silly, T. Lannuzel, F. Domingues Dos Santos and B. Ameduri, *Macromolecules*, 2017, **50**, 503–514.
63 T. Soulestin, V. Ladmiral, T. Lannuzel, F. Domingues Dos Santos and B. Améduri, *Polym. Chem.*, 2017, **8**, 735–747.
64 S. M. Maguire, N. M. Krook, A. Kulshreshtha, C. R. Bilchak, R. Brosnan, A. M. Pana, P. Rannou, M. Maréchal, K. Ohno, A. Jayaraman and R. J. Composto, *Macromolecules*, 2021, **54**, 797–811.
65 R. Zhang, B. Lee, M. R. Bockstaller, S. K. Kumar, C. M. Stafford, J. F. Douglas, D. Raghavan and A. Karim, *Macromolecules*, 2016, **49**, 3965–3974.
66 S. Virtanen, T. Krentz, J. Nelson, L. Schadler, M. Bell, B. Benicewicz, H. Hillborg and S. Zhao, *IEEE Trans. Dielectr. Electr. Insul.*, 2014, **21**, 563–570.
67 R. I. Mahdi and W. H. A. Majid, *RSC Adv.*, 2016, **6**, 81296–81309.
68 A. Ferri, S. Barrau, R. Bourez, A. Da Costa, M. H. Chambrier, A. Marin, J. Defebvin, J. M. Lefebvre and R. Desfeux, *Compos. Sci. Technol.*, 2020, **186**, 107914.
69 C. Xu, K. Ohno, V. Ladmiral and R. J. Composto, *Polymer*, 2008, **49**, 3568–3577.
70 H. Chao and R. A. Riggleman, *Polymer*, 2013, **54**, 5222–5229.
71 S. K. Kumar, N. Jouault, B. Benicewicz and T. Neely, *Macromolecules*, 2013, **46**, 3199–3214.